P5.6 **Generation of Eddy Dissipation Rate Map at the Hong Kong International Airport Based on Doppler LIDAR Data**

P.W. Chan *
Hong Kong Observatory, Hong Kong, China

1. INTRODUCTION

The Hong Kong International Airport (HKIA) is located to the north of the mountainous Lantau Island (Figure 1), which has peaks reaching nearly 1000 m AMSL and valleys as low as 300 m. Winds blowing from east to southwest may be disrupted after climbing over this complex terrain, resulting in turbulent airflow over HKIA. Such cross-mountain winds are most common in spring-time when the northeast monsoon brings east to southeasterly winds to the south China coast, and in the summer when Hong Kong is under the influence of tropical cyclones or the southwest monsoon.

In accordance with the practice of the International Civil Aviation Organization (ICAO), turbulence intensity is expressed in terms of the eddy dissipation rate (EDR). Since the opening of the present HKIA, on average 1 in about 2000 flights reports the encounter of significant turbulence, which includes moderate turbulence (EDR between 0.3 and 0.5 $m^{2/3}s^{-1}$) and severe turbulence (EDR of 0.5 $m^{2/3}s^{-1}$ or above).

The Hong Kong Observatory (HKO) operates a Windshear and Turbulence Warning System (WTWS) to provide automatic turbulence alerting service at HKIA (see, e.g. Chan and Chan 2004, for a brief introduction to WTWS). WTWS mainly makes use of the wind measurements from a network of ground-based anemometers to estimate the turbulence intensity along the flight paths. Data from a Terminal Doppler Weather Radar are also considered, but they are assigned with a smaller weight (0.2, compared to 0.8 of the anemometer-based EDR estimate). A study has also been conducted on the quality of EDR estimates from two boundary layer wind profilers on Lantau Island for turbulence detection at HKIA (Chan and Chan 2004).

The above methods are based on meteorological data that are collected outside the flight paths of HKIA. The operation of a Doppler LIght Detection And Ranging (LIDAR) system by HKO at HKIA (Figure 1) opens up an opportunity to directly measure the radial component of the wind in high spatial resolution and thus the turbulence intensity at locations sufficiently close to the flight paths. An experiment was performed in 2004 to examine the quality of LIDAR-based EDR estimates from a one-dimensional staring laser beam (Chan et al. 2005). The present study extends this work by calculating the two-dimensional "EDR map" based on the velocity data from a scanning laser beam, with the ultimate goal of monitoring the turbulence intensity along all the flight paths of HKIA.

* *Corresponding author address:* P.W. Chan, Hong Kong Observatory, 134A Nathan Road, Hong Kong email: pwchan@hko.gov.hk

Figure 1 Map of HKIA and Lantau Island (height contours: 100 m). Locations of the LIDAR and the sonic anemometer used for this study are indicated by red dots.

This paper is organized as follows. Section 2 gives an overview of the methodology to calculate the EDR map. Section 3 provides two examples of the map, one for east to southeasterly winds in spring-time and another for a tropical cyclone case. It also discusses the quality of the LIDAR-based EDR by comparing with the EDR values from a 3-D sonic anemometer (RM Young model 81000) installed on top of a small hill (with a height of 166 m AMSL) on the downwind coast of Lantau Island (Figure 1). Conclusions and suggestions for further studies are given in Section 4.

2. CALCULATION OF EDR MAP

The LIDAR at HKIA is located at about 50 m AMSL on top of a building. It uses a 2-micron laser beam to measure the radial component of the wind up to about 10 km, with a horizontal resolution of 105 m. It repeats a number of scans within 2 – 6 minutes (depending on the implemented scan strategy), including three Plan-Position Indicator (PPI) scans at the elevation angles of 0 (i.e. horizontal), 1 and 4.5 degrees, Range-Height Indicator (RHI) scans and glide path scans (Chan et al. 2006). As a start, the present study only focuses on the 0 and 1 degree PPI scans, which are rather close to the aircraft approach paths.

Quality control of the LIDAR's velocity data is critical to calculate turbulence intensity because the velocity structure function (Eq. (2) below) is very sensitive to the presence of even a single piece of erroneous velocity measurement that deviates significantly from the radial velocities at the adjacent range gates. Such erroneous data may arise from reflection of the laser beam by hard targets (stationary or moving) and deterioration of the laser optics (laser diodes, optical amplification components, etc.). Besides the implementation of clutter maps and the automatic signal-to-noise threshold (which are

standard features of the LIDAR equipment), additional quality control measures that have been adopted for the windshear detection algorithm (Chan et al. 2006) are applied to the LIDAR's velocity data in this paper.

The EDR is calculated using the structure function approach. The temporal fluctuation method originally developed for a staring laser beam (Frehlich et al. 1998) cannot be adopted here because the PPI scans are only updated every several minutes. The spatial fluctuation method is used instead. For the case of a staring beam, it has been found to give EDR values comparable to those determined from the temporal fluctuation method (Chan et al. 2005).

The whole PPI scan area consists of two fan-shaped sectors, as shown, for example, in Figures 4 and 9. This is not a full circular disk due to blockages by nearby buildings/terrain and sector blanking from laser safety consideration. The whole area is first divided into a number of smaller sectors, each with a range of about 1 km (i.e. 10 range gates) and an azimuthal span of 20 degrees (which includes 20 beams or so). For a particular scan k, the radial velocity "surface" within this sector (as a function of range R and azimuth θ) is fitted with a (normally slanting) plane using singular value decomposition method. The velocity fluctuation $\hat{v}'$ at each point in space (R, θ) is taken to be the difference between the measured radial velocity $\hat{v}$ and the fitted velocity $\bar{v}$ on the plane:

$$\hat{v}'(R,\theta,k) = \hat{v}(R,\theta,k) - \bar{v}(R,\theta,k) \,. \qquad (1)$$

The velocity structure function for two ranges R_1 and R_2 of each small sector is calculated by:

$$\hat{D}_v(R_1,R_2) = N^{-1}\sum_{\theta,k}\left[\hat{v}(R_1,\theta,k) - \hat{v}(R_2,\theta,k)\right]^2 - \hat{\sigma}^2_{\Delta e}(R_1,R_2) \,. \qquad (2)$$

where the summation is made over all the azimuth angles θ of the small sector and the scans k in the period under consideration (which is taken to be 30 minutes in order to make sufficient number of observations of turbulent eddies for an accurate ensemble average), N is the total number of velocity fluctuation pairs in the summation, and the last term on the right hand side of Eq. (2) is an estimation of the error associated with random fluctuations of the LIDAR signal.

Following Frehlich et al. (1998), one way to calculate the error term is to look at the spectral density of the velocity fluctuation difference:

$$\overset{\Lambda}{\Phi}_{\Delta v}(\theta^{-1},R_1,R_2) = \frac{\Delta\theta}{N_1}\left|P(\theta^{-1}/\Delta(\theta^{-1}),R_1,R_2)\right|^2 \qquad (3)$$

where

$$P(j,R_1,R_2) = N_2^{-1}\sum_{l=0}^{N_1-1}\sum_{k=1}^{N_2}(\hat{v}'(R_1,l\Delta\theta,k) - \hat{v}'(R_2,l\Delta\theta,k))$$
$$x\exp(-2\pi ijl/N_1) \,. \qquad (4)$$

In the above equation, N_1 is the number of azimuth angle increment $\Delta\theta$ in the small sector (so that N_1 times $\Delta\theta$ is the azimuthal angular range of this sector),

N_2 is the number of scans in the 30-minute period, $i = \sqrt{-1}$, and $\Delta(\theta^{-1}) = 1/(N_1\Delta\theta)$. The use of the azimuth angle as the variable in the discrete Fourier transform of the velocity fluctuation difference is basically equivalent to using time (the normal convention) if the azimuthal scan rate of the laser beam is more or less constant. Averaging over different scans is performed in order to accumulate sufficient number of velocity fluctuation differences in the calculation of the spectral density; otherwise the spectral density may show up significant variations as a function of θ^{-1} due to limited sample size.

An example of the calculated spectral density is given in Figure 2. The noise floor at high θ^{-1} (or high frequency) is not apparent, probably due to the rather low noise of the laser (as also discussed in Chan et al. 2005) and the small number of azimuth angle increments (20 or so) in each small sector. Determination of the error term from spectral density in spatial fluctuation calculation method could be investigated further by scanning the laser beam more slowly (the present azimuthal scan rate of the LIDAR is in the order of 15 degrees/second). However, with a single LIDAR only, there is a compromise among spatial resolution (e.g. for estimating the error term), spatial coverage (how large the area one likes to study the turbulence intensity) and temporal resolution (in view of the high temporal variability of turbulence phenomenon). This issue would be considered in a separate study. In the present paper, the error term in Eq. (2) would be ignored.
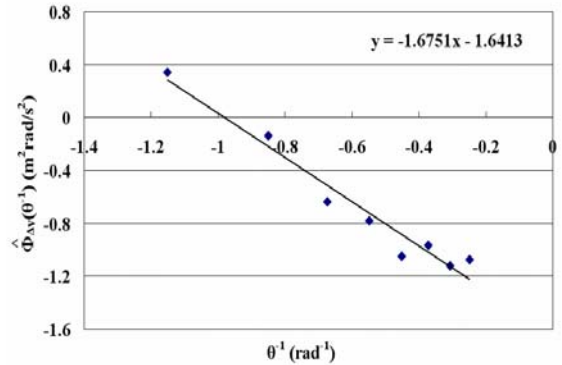

Figure 2   Log-log plot of the spectral density for the velocity fluctuation difference between the ranges 3489 and 3804 m over the small sector centred at the azimuth angle 235°, in the period 12:45 to 13:15 UTC, 24 March 2004.

Another challenge for accurate determination of EDR using a scanning laser beam is the correction for transverse-dimension velocity averaging, especially at longer ranges (Hannon et al. 2005). There are no established methods to calculate the correction. This factor is not considered in the present study.

The calculated velocity structure function is fitted with the von Kármán model to determine the EDR (Frehlich and Cornman 2002).

3.   EXAMPLES OF LIDAR-BASED EDR

3.1   Spring-time case: 23 – 25 March 2004

In the morning of 24 March 2004 (Figure 3, Hong Kong time = UTC + 8 hours), synoptically a

ridge of high pressure over the southeastern coast of China brought an easterly airstream to Hong Kong. As shown in the LIDAR's velocity data in the 0-degree PPI scans (Figure 4(a)), the wind was mainly from the east, with a slight southerly component. The maximum radial velocity was about 10 ms^{-1}. The EDR calculated from these scans (Figure 4(b)) was generally small in the vicinity of HKIA at that time, in the order of 0.15 m$^{2/3}$s^{-1} or less (light and dark blue).
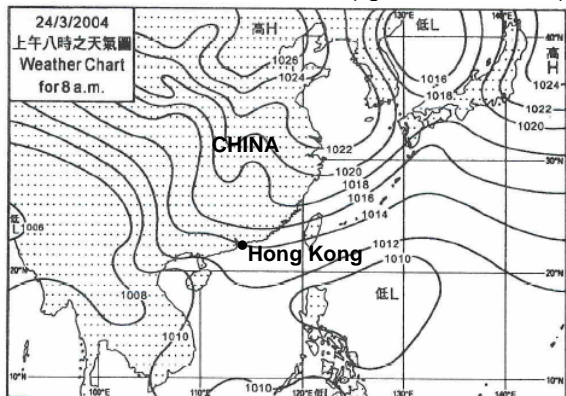

Figure 3   Surface isobar chart at 8 a.m., 24 March 2004.

There were a few localized regions with higher EDR values. For instance, EDR reached about 0.35 m$^{2/3}$s^{-1} persistently to the east-northeast of the LIDAR just beyond its blind zone. The EDR map gives a general indication about the spatial variability of turbulence intensity.

Though stringent quality-control measures have been applied to the raw velocity data (Section 2), some pieces of erroneous data are still present at far ranges of the LIDAR, resulting in unrealistically large EDR values (sometimes could be close to unity). This shows up as "arcs" of red or yellow in the EDR map (Figure 4(b)). The incorrect EDR values could be removed by imposing spatial and temporal continuity on the EDR map using some tuned thresholds and, more fundamentally, applying additional quality-control measures to the raw velocity data. These methods would be considered in future studies.

Later on that day, the wind picked up and veered gradually to gain a more southerly component. Accelerated flows emanating from the valleys of Lantau Island became more apparent (Figure 4(c)). Compared to the situation in the morning, the EDR
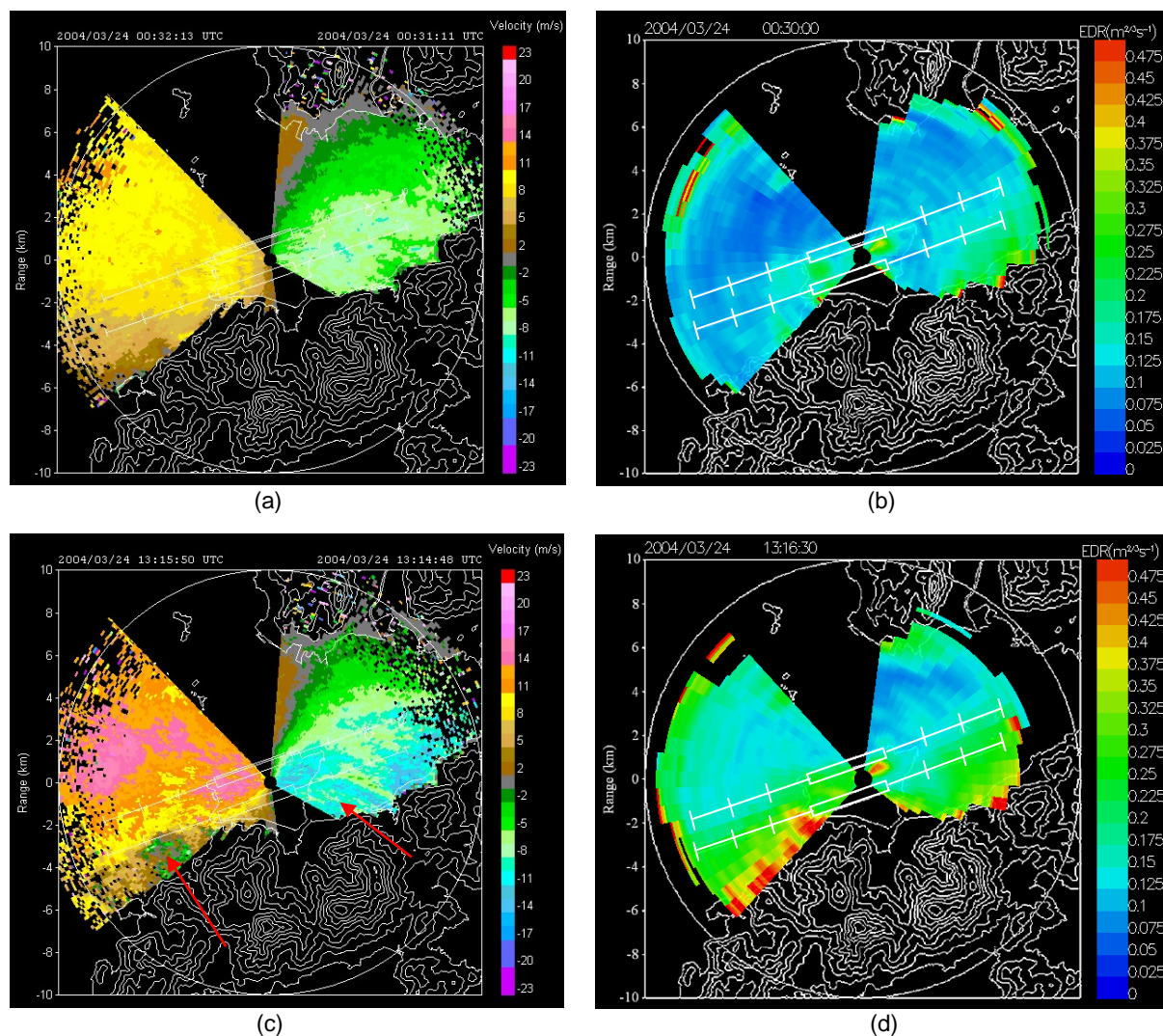

(a)

(b)

(c)

(d)

Figure 4   Radial velocity imagery (left hand side) and EDR map (right hand side) obtained from 0-degree PPI scans of the LIDAR at about 00:30 UTC ((a) and (b)) and 13:16 UTC ((c) and (d)) of 24 March 2004.   The major valley flows from Lantau Island are indicated by red arrows in (c).

was generally higher in the vicinity of HKIA (Figure 4(d)) as a result of higher wind speed and disruption of the more southerly airflow by Lantau terrain. It was in the order of 0.3 $m^{2/3}s^{-1}$ or above within the first 2 km or so downstream of Lantau Island and gradually decreased northwards over the sea. Moreover, the EDR was generally higher (exceeding 0.5 $m^{2/3}s^{-1}$) just downstream of the Lantau terrain to the west of the LIDAR compared with similar locations to the east of the LIDAR. These regions of higher EDR appear as "flares of red" emanating from the terrain in Figure 4(d). The more turbulent airflow over there may be related to the convergence between the prevailing easterly over HKIA and the southerly valley flow from Lantau Island (Figure 5) (Chan and Mok 2004) and jump/mountain wake in the valley flow (Szeto and Chan 2006). The cause of the turbulent flow would be studied in the future.
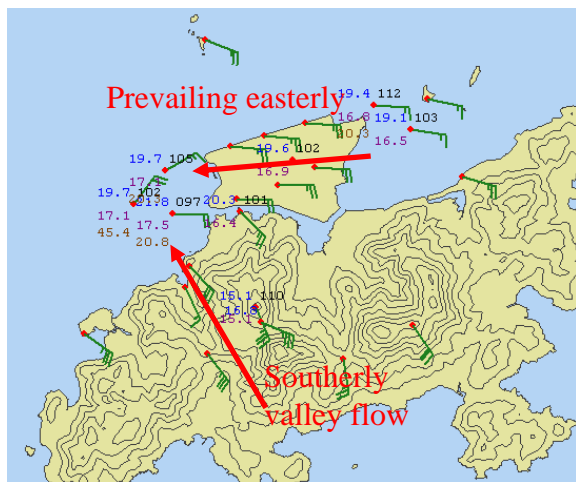

Figure 5   Surface wind observations in the vicinity of HKIA at 13:16 UTC, 24 March 2004.

To examine the quality of the LIDAR-based EDR estimates, they are compared with the EDR values calculated from the wind velocity measurements (at 20 Hz output) of a 3-D sonic anemometer on Lantau Island (see Figure 1 for location). The EDR calculation method is similar to that in a past experiment performed on a rather flat area (Chan 2004). However, since the anemometer in this case is mounted on top of a conical hill, the vertical velocity is not always negligible in comparison to the horizontal wind speed. In fact, it is not uncommon to have an upward velocity of several metres per second in strong east to southeasterly wind situation as the wind climbs over the hill. Following the common practice, co-ordinate transformation is applied to the three components of the wind to align the longitudinal axis with the mean wind direction.

Figure 6 shows the time series of the EDR values calculated from the sonic anemometer and the LIDAR measurements (at the location closest to the anemometer) on 24 March 2004. Both datasets have a similar temporal trend, viz. the turbulence intensity generally increases in the course of the day.

The scatter plot of the EDR calculated from the vertical velocity data of the sonic anemometer and that from the 1-degree PPI scans of the LIDAR at the location nearest the anemometer is shown in Figure 7, with the y-intercept set to be zero. The 1-degree PPI

scans are chosen because the height of the laser beam at the anemometer's location (137 m AMSL) is close to that of the anemometer itself (176 m AMSL). The plot covers the period 23 – 25 March 2004. Both EDR values are determined over 30-minute periods. The slope of the least-square linear fit to the data points is close to unity. The correlation coefficient between the two datasets exceeds 0.9, which is considered very high judging from the fact that the EDR from the sonic anemometer is essentially a point measurement whereas the corresponding value from the LIDAR represents the turbulence over a much larger area (1 km in range and 20 degrees in azimuth).
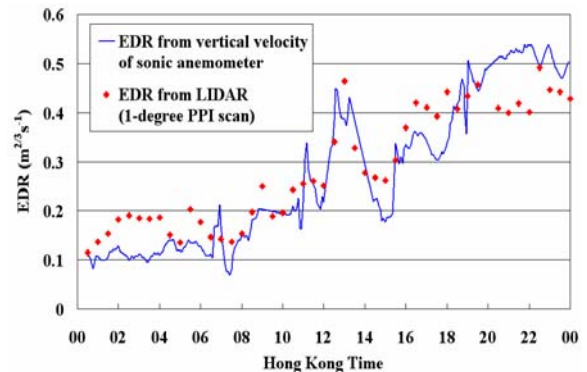

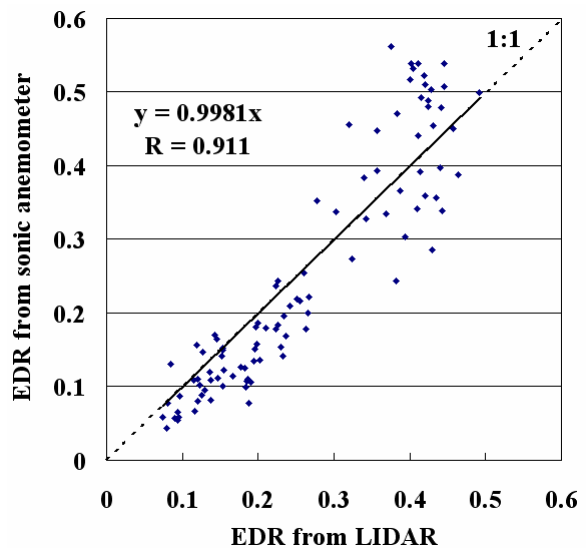Figure 6   Time series of the EDR calculated from the sonic anemometer and the LIDAR on 24 March 2004.

Figure 7   Scatter plot of the EDR from the sonic anemometer and the LIDAR in the period 23 – 25 March 2004.

Wind component of the sonic anemometer to calculate EDR	Slope	Correlation coefficient (R)
Vertical	0.9981	0.911
Longitudinal	1.1274	0.903
Transverse	0.9177	0.887

Table 1: Slope (m) and correlation coefficient of the least square linear fit (y = m*x) between the EDR derived from different wind components of the sonic anemometer (y) and that calculated from 1-degree PPI scan of the LIDAR (x) at the anemometer's location.

Table 1 summarizes the slopes and correlation coefficients of the least-square linear fits (with y-intercepts set to be zero) between the EDR determined from each of the three components of the wind data of the sonic anemometer and that from the 1-degree PPI scans of the LIDAR.   The slopes are close to unity and the correlation coefficients are about 0.9 in all cases.   The sonic anemometer is situated at about 5 km from the LIDAR, which is half of the LIDAR's maximum measurement range.   From the present results, it shows that the effect of velocity averaging of the LIDAR in the longitudinal and transverse dimensions on EDR estimation (Hannon et al. 2005) is not significant, at least at this range from the LIDAR.

Based on the slopes of the above least-square linear fits, the ratio of the EDR in the vertical to longitudinal to transverse components is 1.0:1.1:0.9.   Thus on average, the turbulence at the location of the sonic anemometer is close to isotropic.

3.2   Typhoon case: 23 – 27 August 2003

Typhoon Krovanh tracked west-northwestwards across the northern part of South China Sea in late August 2003 (Figure 8).   It brought east to southeasterly winds up to storm force to Hong Kong.   For instance, at about 1:30 a.m. of 25 August 2003 (17:30 UTC of 24 August), 1-degree PPI scans of the LIDAR gave radial velocities close to 20 m/s in the vicinity of HKIA (Figure 9(a)).   Because of the high humidity of the air, the measurement range of the LIDAR was reduced.   There were not much velocity data beyond 8 km or so to the west of the LIDAR.

Similar to the above spring-time case, the airflow seems to be more turbulent in the areas just downstream of the Lantau terrain to the west of the LIDAR compared with the corresponding locations east of the LIDAR, as revealed by the presence of many small-scale features (with horizontal dimensions of several hundred metres) in the radial velocity imagery (Figure 9(a)).   This pattern is also confirmed from the EDR map (Figure 9(b)).   Once again, "flares" of high EDR values (around 0.5 $m^{2/3}s^{-1}$) emanate from the Lantau terrain to the southwest of LIDAR.   They are more extensive in size compared to the spring-time case and affect almost the whole western approach corridor of the south runway, but the relatively less turbulent region between 1 and 2 nautical miles from the runway threshold deserves more in-depth studies.
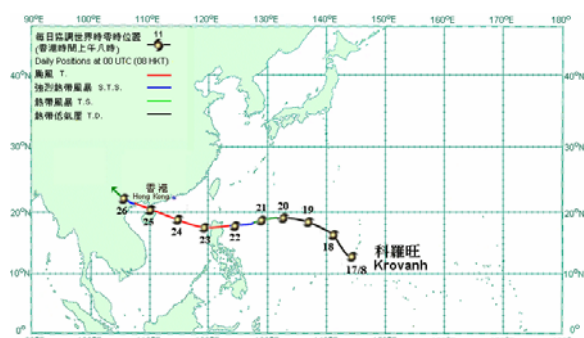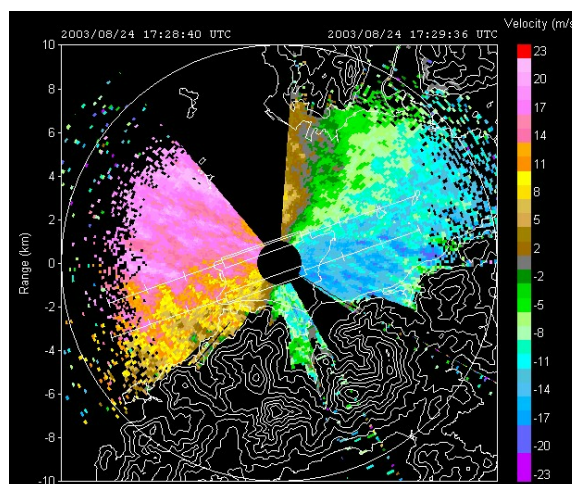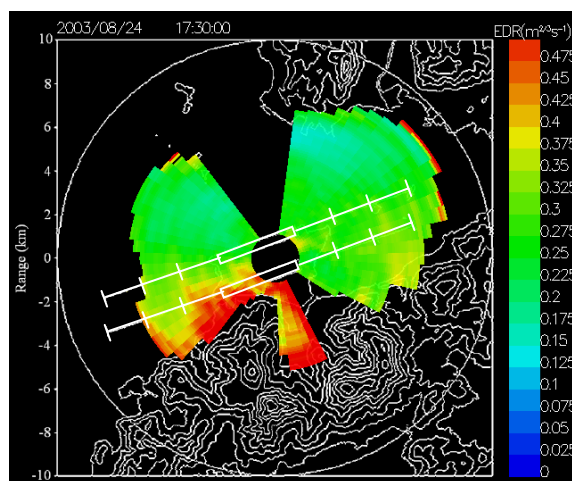

Figure 8   Track of Typhoon Krovanh.   The dots refer to locations of Krovanh at 8 a.m. (00 UTC) of the dates (the numbers next to the dots) in August 2003.

(a)

(b)

Figure 9   Radial velocity imagery from 1-degree PPI scan of the LIDAR (a) and the EDR map (b) at around 17:30 UTC, 24 August 2003.

The EDR determined from 1-degree PPI scans of the LIDAR is again compared with those calculated from the three components of the wind measurements of the sonic anemometer.   Results for the period 23 – 27 August 2003 are summarized in Table 2.   Compared to the spring-time case, the slopes deviate slightly more from unity and the correlation coefficients are generally smaller, but still reach at least 0.92 and 0.8 respectively.   The calculation of EDR in the typhoon case is more challenging because of the limited measurement range of the LIDAR and the missing/erroneous wind data from the sonic anemometer in episodes of heavy rain.   Given that, the present comparison results are considered to be satisfactory.

Wind component of the sonic anemometer to calculate EDR	Slope	Correlation coefficient (R)
Vertical	0.9283	0.851
Longitudinal	0.9881	0.799
Transverse	0.9247	0.839

Table 2: Same as Table 1, but for the period 23 – 27 August 2003.

Based on the slopes in Table 2, the ratio of the

EDR in the vertical to longitudinal to transverse components is about 1.0:1.1:1.0. The turbulence at the location of the sonic anemometer is close to isotropic.

4. CONCLUSIONS

Two-dimensional EDR maps were calculated from radial velocities measured in PPI scans of the LIDAR at HKIA. The whole scanning area was divided into a number of small sectors, each with a range of about 1 km and an azimuthal span of 20 degrees. The radial velocity "surface" as a function of range and azimuth in each scan was fitted with a slanting plane to calculate the velocity fluctuation with respect to this fitted plane. The velocity structure function was calculated from velocity fluctuations at different lag distances and compared with the von Kármán model to determine the EDR.

Some interesting features were revealed in the EDR maps for the two typical cases of turbulent airflow over HKIA, namely, a spring-time southeasterly wind episode and a typhoon case. Areas of high EDR were observed downstream of the Lantau terrain to the west of the LIDAR. They were related to airflow disruption by the hills (e.g. in the form of jump and mountain wake) as well as convergence between the prevailing east to southeasterly and the southerly gap flow emanating from Lantau Island.

The quality of the LIDAR-based EDR was studied by comparing with the EDR values calculated from the 3-D wind measurements by a sonic anemometer located on top of a small hill on the downwind coast of Lantau Island. The two sets of EDR are found to correlate well in general. The proportionality factor between them is close to unity. These results are satisfactory considering that the sonic anemometer made a point measurement whereas the LIDAR-based EDR was calculated from radial velocity data over a much larger area.

Future studies on the EDR map would include:

(a) calculation of EDR map using glide-path scans of the LIDAR (Chan et al. 2006) to see how the LIDAR-based EDR values compare with those estimated from the onboard Flight Data Recorder (FDR) data of aircraft;
(b) reduction of the period for calculating EDR (currently 30 minutes) with more dedicated scans of the LIDAR over a single runway;
(c) improvement of the quality of EDR map by removing the erroneous EDR values due to data quality issues (discussed in Section 3);
(d) estimation of the error term in the velocity structure function (Eq. (2), as discussed in Section 2); and
(e) calculation of EDR map using RHI scans of the LIDAR to study the vertical distribution of turbulence intensity.

References

Chan, P.W., 2004: Measurement of eddy dissipation rate by a mini-sodar for aviation application: comparison with tower measurement. *11th Conference on Aviation, Range, and Aerospace Meteorology*, American Meteorological Society, Massachusetts (on-line proceedings).

Chan, P.W., and S.T. Chan, 2004: Performance of eddy dissipation rate estimates from wind profilers in turbulence detection. *11th Conference on Aviation, Range, and Aerospace Meteorology*, American Meteorological Society, Massachusetts (on-line proceedings).

Chan, P.W., K.K. Lai and C.M. Shun, 2005: Measurement of turbulence in terrain-disrupted airflow at the Hong Kong International Airport using a Doppler LIDAR. *Croatian Meteorological Journal, 40,* 503-506.

Chan, P.W., C.M. Shun and K.C. Wu, 2006: Operational LIDAR-based system for automatic windshear alerting at the Hong Kong International Airport. *12th Conference on Aviation, Range, and Aerospace Meteorology*, American Meteorological Society, Georgia (on-line proceedings).

Chan, S.T., and C.W. Mok, 2004: Comparison of Doppler LIDAR observations of severe turbulence and aircraft data. *11th Conference on Aviation, Range, and Aerospace Meteorology*, American Meteorological Society, Massachusetts (on-line proceedings).

Frehlich, R., and L. Cornman, 2002: Estimating spatial velocity statistics with coherent Doppler Lidar. *J. Atmos. Oceanic Technol.*, **19**, 355–366.

Frehlich, R., S.M. Hannon and S.W. Henderson, 1998: Coherent Doppler Lidar measurements of wind field statistics. *Bound.-Layer Meteor.*, **86**, 233–256.

Hannon, S. M., J.V. Pelk and P. Benda, 2005: Autonomous Doppler Lidar wind and aerosol measurements for Pentagon Shield. *2nd Symposium on Lidar Atmospheric Applications*, American Meteorological Society, California (on-line proceedings).

Szeto, K.C., and P.W. Chan, 2006: High resolution numerical modelling of windshear episodes at the Hong Kong International Airport. *12th Conference on Aviation, Range, and Aerospace Meteorology*, American Meteorological Society, Georgia (on-line proceedings).